Efficient *Escherichia coli (E. coli)* Trapping and Retrieval from Bodily Fluids via a Three-Dimensional (3D) Microbeads Stacked Nano-Device

Xinye Chen,[1,2] Abbi Miller,[3] Shengting Cao,[4] Yu Gan,[4] Jie Zhang,[5] Qian He,[2,6] Ruo-Qian Wang,[7] Xin Yong,[8] Peiwu Qin,[6] Blanca H. Lapizco-Encinas,[3] and Ke Du [1, 2 *]

[1] Department of Microsystems Engineering, Rochester Institute of Technology, Rochester, NY 14623, United States
[2] Department of Mechanical Engineering, Rochester Institute of Technology, Rochester, NY 14623, United States
[3] Department of Biomedical Engineering, Rochester Institute of Technology, Rochester, NY 14623, United States
[4] Department of Electrical and Computer Engineering, University of Alabama, Tuscaloosa, AL 35401, United States
[5] Carollo Engineers, Inc., Seattle, WA 98101, USA
[6] Center of Precision Medicine and Healthcare, Tsinghua-Berkeley Shenzhen Institute, Shenzhen, Guangdong Province 518055, China
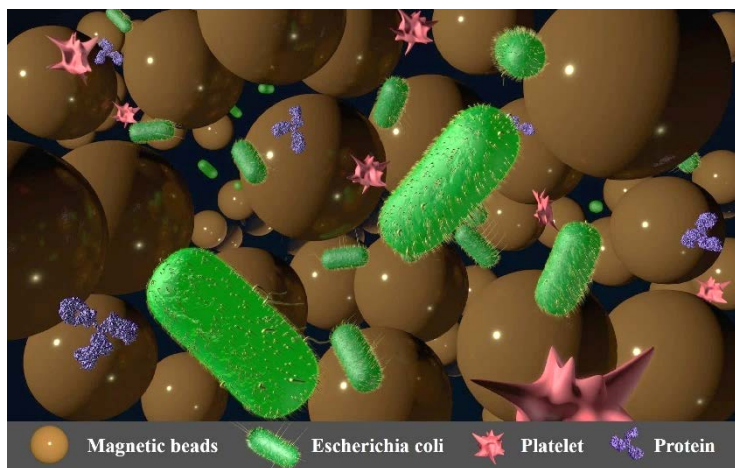[7] Department of Civil and Environmental Engineering, Rutgers, The State University of New Jersey, NJ 08854, USA
[8] Department of Mechanical Engineering, The State University of New York, Binghamton, NY 13902, USA

Contact: ke.du@rit.edu

ABSTRACT

A micro- and nano-fluidic device stacked with magnetic beads is developed to efficiently trap, concentrate, and retrieve *Escherichia coli* (*E. coli*) from bacteria suspension and pig plasma. The small voids between the magnetic beads are used

to physically isolate the bacteria in the device. We use computational fluid dynamics (CFD), 3D tomography technology, and machine learning to probe and explain the bead stacking in a small 3D space with various flow rates. A combination of beads with different sizes is utilized to achieve a high capture efficiency of ~86% with a flow rate of 50 µL/min. Leveraging the high deformability of this device, the *E. coli* sample is retrieved from the designated bacteria suspension by applying a higher flow rate, followed by rapid magnetic separation. This unique function is also utilized to concentrate *E. coli* from the original bacteria suspension. An on-chip concentration factor of ~11× is achieved by inputting 1,300 µL of the *E. coli* sample and then concentrating it in 100 µL buffer. Importantly, this multiplexed, miniaturized, inexpensive, and transparent device is easy to fabricate and operate, making it ideal for pathogen separation in both laboratory and point-of-care (POC) settings.

KEYWORDS – *Escherichia coli (E. coli), magnetic bead, nano-sieve, computational fluid dynamics (CFD), optical tomography, machine learning, point-of-care (POC)*

Inadequate water supplies and poor sanitation in low- and middle-income settings have elevated the global concerns for waterborne disease outbreaks. In 2012, over 500,000 people died due to diarrhea contamination of drinking water.[1] Microorganisms such as *Escherichia coli* (*E. coli*) can cause fecal contamination in recreational and drinking water and post a high risk of disease transmission. The U.S. Centers for Disease Control and Prevention (CDC) reported that over 70,000 distinct illnesses caused by *E. coli* occur each year, resulting in more than 2,000 hospitalizations.[2] While *E. coli* infection can be treated with common antibiotics, some strains of this bacteria have developed resistance to antibiotics, leading to longer recovery times and even death. As the development of new antibiotics is slow and challenging, drug-resistant bacteria are gradually becoming one of the leading public health concerns. Currently, around 700,000 people are killed each year due to antibiotic-resistant infections. Projected analysis indicates that if no action is taken to reverse this trend, the global mortality rate caused by drug-resistant bacteria could rise to 10 million each year worldwide, leading to an annual loss of 100 trillion USD.[3,4]

The study of drug-resistant strains requires bacteria isolation, purification, concentration, followed by molecular characterization such as polymerase chain reaction (PCR),[5,6] enzyme-linked immunosorbent assay (ELISA),[7,8] cell plating,[9,10] and microscopy.[11,12] The rapid identification of drug-resistant bacteria allows physicians to prescribe a viable drug initially, resulting in a better prognosis for the patient and increasing the likelihood of survival. ELISA microarrays can be used to isolate target bacteria by specific antibody.[13] However, the capture efficiency is low, and impurities found in bodily fluids can inhibit antibody activity.[14] Membrane-based filtration has been widely utilized and is advantageous because of cost-effectiveness, simplicity, and rapidness.[15] However, the captured bacteria need to be retrieved from the membrane by iterative buffer washing, which could result in undesired dilution.[16] For instance,

100 colony-forming unit (CFU)/mL of *E. coli* in drinking water can cause various infections, including urinary tract infections and diarrhea.[17] Therefore, retrieving the bacteria in a small volume is required to increase the sample concentration for detection. Besides, membrane-based filtration is more problematic when dealing with blood samples, as multiple filters with various pore sizes are needed to reduce clogging issues with the white blood cells and red blood cells.[18,19] Cell leakage is another challenge as the bacteria can deform to pass through the pores. In recent years, microfluidics-based approaches, such as inertial force separation,[20,21] hydrodynamic separation,[22,23] electrophoresis,[24,25] and acoustics separation,[26,27] have been developed to efficiently separate and detect pathogens; however, all of these methods have limitations, either require sophisticated microfluidic designs or complicated instruments. Therefore, physical barriers such as "T-junction" [28,29] and micro-obstacle arrays[30,31] were introduced to capture the cells from bodily fluids; yet, most of the bacteria sizes range between 0.5 to 5 µm, making the fabrication process challenging.[32]

We previously developed a deformable nano-sieve device for rapid and size-selective separation of microplastics.[33] Deformation of this device was regulated by flow rate, thus allowing efficient particle trapping and releasing. Exploiting highly efficient particle trapping of the nano-sieve, stacking of the beads is achieved by hydrodynamic flow with various flow rates, and the liquid-flow profile of the stack is imaged by optical coherence tomography.[34] Then, a novel machine learning method is applied to automatically reconstruct 3D topology within the device.[35] Our system can isolate and concentrate *E. coli* cells from either bacteria suspension or pig plasma by physically capturing the bacteria in the beads assay. Remarkably, the captured bacteria are easily released from the device with flow rate induced channel deformation, followed by bead isolation with a magnetic. An on-chip concentration factor of ~11 times is achieved by concentrating the

bacteria in 100 µL buffer from a 1,300 µL original sample. By using this method, intact bacteria can be rapidly collected from patient samples for down-stream molecular diagnosis and imaging. More importantly, multiple nano-sieve devices can be patterned on a small chip by using standard microfabrication techniques and operated by a small syringe pump, leading to a simple, inexpensive, and multiplexed instrument for bacteria sample preparation, intended for point-of-care (POC) settings.

Results

Our method for bacteria isolation and retrieval is presented in **Fig. 1a**. Magnetic beads with a diameter ranging from 2.8 to 10 µm are pumped into the nano-sieve device at a flow rate of 50 µL/min. Beads with a large volume are stacked tightly within the 3D space (**Fig. 1a-i**). Then, the bacterial solution is pumped into the bead-stacked channel, and the bacteria are captured in the bead assay as the buffer filtered into the waste reservoir (**Fig. 1a-ii**). As the bacteria continue to pass through the nano-sieve device, an accumulation of trapped cells occurs in the 3D space. Finally, a high flow rate is applied to heave the nano-sieve and release the beads/bacteria mixture (**Fig. 1a-iii**) to the assigned reservoir (Eppendorf tube). To fabricate the nano-sieve device, standard photolithography and wet etching techniques were used to pattern a rectangular feature on tetraethyl orthosilicate (TEOS) (L: 8 mm; W: 2 mm). Then, a thin layer of positive photoresist (PR) with a thickness of ~1 µm was coated uniformly on the substrate and patterned by photolithography. This resulted in PR coverage in the trench of TEOS. The nano-sieve channel was sealed by bonding it to a flat Polydimethylsiloxane (PDMS) sheet (5 mm), followed by acetone rinsing. The on-chip experiment setup is shown in **Fig. 1b-i**. The magnetic beads and bacteria are pumped into the nano-sieve by a multi-channel syringe pump. A magnetic rack rapidly separated

the mixture of released beads/bacteria. A scanning electron microscope (SEM) was used to characterize beads stacking within the nano-sieve device (**Fig. 1b-ii to Fig. 1b-iv**). The beads are uniformly stacked and heaved the nano-sieve into an arch shape. We used fluorescence microscope to image the entire nano-sieve device before (**Fig. 1c**) and after (**Fig. 1d**) bacteria-trapping. As shown in **Fig. 1d**, stained bacteria are trapped within the interspaces of the beads assay.

The beads stacking process with a flow rate of 40 µL/min is shown in **Fig. 2a**. Initially (0 s), the nano-sieve is empty (**Fig. 2a-i**). Under the filling process (24 s), the beads begin to stack and form an arch shape (**Fig. 2a-ii**). However, as the pressure drop builds up in the nano-sieve (48 s), beads are pushed to the sides of the channel and burst out to the outlet from the central path of the channel (**Fig. 2a-iii**). This process also moves the beads pack closer to the outlet. As the channel deformation is smaller at the outlet, further filling the beads (72 s) into the device does not burst, and a denser bead stacking in the 3D space is achieved (**Fig. 2a-iv**). The video of this process is shown in Movie S1. To understand this time-dependent process, we developed a computational fluid dynamics (CFD) model to study the magnetic bead transport in the deformed nano-sieve. We assume that the deformation of the PDMS roof is dominated by pumping pressure and that the effect of the stacked bead and heaving on the roof is negligible. **Fig. 2b-i** depicts flow rate of 20 µL/min, the highest flow velocity in the channel is 0.035 m/s, and the maximum height in the channel is 19 µm at the middle cross-sectional (Y-Z) plane. The velocity at the centroid of the channel increases with the increased flow rate (**Fig. 2b-i to Fig. 2b-iv**). At a flow rate of 50 µL/min, the highest flow rate is 0.055 m/s, and the maximum height is 30 µm at the middle cross-sectional plane. This high flow rate and large deformation of the channel cause the beads moving to the sides of the channel and to the outlet reservoir. This result matches our experimental observation and can explain the initial beads stacking and burst process (see. **Fig. 2a-i** to **Fig. 2a-iii**).

After the initial burst, the beads move closer to the outlet. Moreover, the inflow of beads starts to the reconstruction of the 3D space, which is further used for bacteria-trapping. We used 3D tomography technology to scan the entire channel after the bead stacking and applied machine learning tools to extract the topology-related data (**Fig. 3a**). The scanning results and quantitative measures of the microbead array are depicted in **Fig. 3a**. An overlay of the 3D mask (in pink) and the raw data are found to be dependent on the flow rate ranging from 20 to 50 µL/min. A mask of bead stacking was generated in each B-scan (the 2D plan along the direction of light propagation) using a K-mean clustering method and morphological operations, as shown in **Fig. 3b**. The white region corresponds to bead stacking, and the black region corresponds to the background and the coverslip. The maximum height of the bead stack was measured from the mask. For each volume, 3D topology was generated by aligning 2D masks in 3D space. The volume of deposited beads and the maximum height versus flow rates are presented in **Fig. 3c**. With a flow rate of 20 µL/min, the total volume and the maximum height in the channel were ~26 mm^3 and ~60 µm, respectively. We found that total volume and maximum height show an uptrend that corresponding to increased flow rate. For example, with a high flow rate of 50 µL/min, the volume and maximum height were increased to ~180 mm^3 and ~130 µm, respectively. As the original channel height was only 200 nm, a ~650× increase of channel height was observed without showing channel failure.

Fig. 4 presents the trapping efficiency and retrieval factor of bacteria in a nano-sieve device. Two hundred microliter of stained bacteria sample (concentration: 1.11E8 CFU/mL) was pumped into the beads-stacked nano-sieve device, and the fluorescence signal of the filtered supernatant was measured by using a spectrofluorometer at an excitation wavelength of 480 nm. By introducing 10 µm magnetic beads in the nano-sieve, the measured relative fluorescence intensity of the filtered supernatant is ~140 counts, demonstrating most of the bacteria (~65%) were trapped

in the nano-sieve device (**Fig. 4a**). Alternatively, the measured fluorescence intensity of the supernatant is only ~30 counts by introducing a bead mixture with various sizes (2.8 µm, 5 µm, and 10 µm), indicating that almost all the bacteria (~92%) were captured in the nano-sieve device. The bacteria-trapping efficiency versus flow rate was then explored. As shown in **Fig. 4b**, without any stacked beads, the bacteria-trapping efficiency is between 18%-38% at flow rates ranging from 8 to 70 µL/min. Adding the beads mixture to the nano-sieve device significantly increases the trapping efficiency. The bacteria-trapping efficiency is above 86% at flow rates of 8-50 µL/min. At a flow rate of 70 µL/min, a bacteria-trapping efficiency of 64% is achieved, which is three times higher than that observed with the nano-sieve device without stacked beads. Following bacteria-trapping, 200 µL phosphate buffered saline (PBS) was pumped into the nano-sieve device at a flow rate of ~900 µL/min. This high flow rate induces significant deformation of the PDMS roof, thus releasing the beads and bacteria into an Eppendorf tube (**Fig. 1b-i** and **Fig. 4c-i**). A fluorescence microscope was used to image the original bacteria sample (**Fig. 4c-ii**), filtered supernatant (**Fig. 4c-iii**), and retrieved sample (**Fig. 4c-iv**). Only a few bacterial cells were observed in the filtered supernatant, again proving negligible bacteria leaking. The retrieved bacteria solution (cells in unit area: 0.142 cells/μm^2) has similar cell numbers to the original sample (cells in unit area: 0.163 cells/μm^2), indicating highly efficient bacterial retrieval. Our platform is capable of trapping and retrieving bacteria from various media, including bodily fluids. We achieve a bacteria-trapping efficiency of ~60% and a retrieval rate of 80% from pig plasma at a flow rate of 8 µL/min (**Fig. 4d**).

   The bead-stacked nano-sieve can be applied to concentrate bacteria samples when the original cell number is low. To explore this, we pumped 1,300 µL bacteria with a concentration of 1.11E7 CFU/mL into the bead-stacked nano-sieve device. Then, we retrieved the bacteria by introducing

100 µL PBS buffer at a flow rate of ~900 µL/min, to obtain an on-chip concentration factor of 13×. As shown in **Fig. 5a**, the original sample with a concentration of 1.11E7 CFU/mL only shows ~60 counts. Notably, the retrieved sample shows fluorescence intensity of ~480 counts, indicating a dramatic increase in sample concentration. The integrated fluorescence signal of **Fig. 5a** with a wavelength from 520-640 nm was plotted and is presented in **Fig. 5b,** showing an excellent linear relationship. A ~11.2× on-chip concentration factor was achieved, which is closely matched to the intended 13× on-chip concentration. This powerful on-chip concentration capability was further confirmed by fluorescence microscopy. The retrieved bacterial sample shows a much higher concentration than the original sample, when compared to the filtered supernatant, indicating an efficient on-chip concentration (**Fig. 5c**).

Discussion

Drug-resistant bacteria have become a severe public health concern. Fortunately, this risk can be reduced via the correct use of prescriptions, and by avoiding unnecessary prescriptions and over-prescription of antibiotics.[36,37] In this regard, rapid isolation of the target bacteria from various samples is an essential step toward the identification of antibiotic resistance and providing early-treatment.[38] Reported here is the development of magnetic beads-stacked nano-sieve device to separate, concentrate, and retrieve bacteria from both buffer solution and pig plasma samples. A high capture efficiency (86%) was achieved at a high flow rate (50 µL/min), indicating that the system can process a large sample volume in a short time for the study of drug-resistant bacteria.

Unlike conventional membrane-based filtration, which is challenging to recover captured pathogens,[39] our system is able to retrieve the captured bacteria into different bacteria suspensions, designed for lysis-free diagnostics.[40] Even though several approaches based on immunoaffinity

separation have been widely used and show high target specificity, they require expensive and delicate antibodies to bind with the surface antigen.[41,42] It also requires time-consuming sample preparation, which is not suitable for POC applications.[43] Our approach entirely relies upon for physical separation, which is robust and does not interfere with the host cellular materials. Furthermore, unlike other microfluidic-based approaches that require complicated instruments and operation,[22,24–27,44–46] our approach only requires a small syringe pump and the miniaturized nano-sieve device, thus it could be used for both lab-based or POC diagnosis.

A unique design that incorporates tightly stacked magnetic beads to trap the bacteria was employed, and the efficiency of bacteria-trapping depends on the configuration of particle stacking. Instead of using complicated micro-and nanofabrication to physically isolate the bacteria,[47,48] our approach simply relies on the beads stacking at various flow rates and does not need expensive and time-consuming nanolithography processes.[49,50] As the beads are pushed to the outlet of the channel, they begin to stack in the 3D space (**Fig. 2a-iv**). The channel height reaches to ~130 µm at 50 µL/min, which is ~650 times higher than the original channel height (~200 nm). This sizeable 3D space created by beads stacking provides numerous voids for bacteria-trapping. This is crucial for bacteria-trapping especially for on-chip concentration, as more voids within the bead array are needed to capture bacteria. Besides, the large strain in the PDMS roof holds the beads array in position. Even with a flow rate at 50 µL/min, we did not observe beads leaking from the nano-sieve, enabling the great capability of processing a large sample volume.

We found that the bead size is also an essential factor for efficient bacteria-trapping. As shown in **Fig. 4**, mixing 5 µm and 2.8 µm beads with the 10 µm beads significantly improves the capture efficiency. Since *E. coli* has a dimension less than 2 µm and has great deformability,[51,52] it can

pass through the small voids at a high flow rate. Thus, we first applied 10 µm beads into the nano-sieve to occupy the 3D space, followed by the application of smaller beads. The tightly stacked small beads array has smaller voids, thus enhancing the bacteria-trapping efficiency. We observed slight reduction of capture efficiency at a flow rate of 70 µL/min due to the bead leaking by the large hydrodynamic deformation. This problem could be easily resolved by designing a multi-channel nano-sieve device to reduce the deformation and beads leaking.

One of the main advantages of microfluidics is the miniaturized size, enabling multi-device operation on a small scale and reducing the consumption of applied samples.[53,54] Leveraging the small size of our nano-sieve device (2 mm × 8 mm), it is possible to pattern hundreds of the nano-sieves on a four inch wafer scale for high throughput multiplexing detection. This can also be used to screen multi-resistant organisms by applying many different antibiotics to isolated samples. The small size of the nano-sieve device also enables us to work with sample volumes ranging from nanoliters to milliliters; thus, it is compatible with either a finger prick test or a blood draw.

A load of drug-resistant bacteria could be as low as ~10-100 CFU/mL in the bodily fluids,[55] thus, concentrating the target is always necessary to reach the detection threshold. By introducing 1,300 µL of the *E. coli* sample into the nano-sieve device and then retrieving the bacteria in 100 µL of the buffer, we demonstrated an on-chip concentration factor of ~11×. Thus, our system is a useful platform for dealing with low concentration samples and could be applied to extend the detection limit. The on-chip concentration factor could be further increased by the application of a larger sample volume and by lowering the volume used for retrieval. By using our novel approach, bacteria could be easily separated, concentrated, and retrieved into any buffer solution and would be available for molecular diagnostic testing of suspects in a POC setting.

Materials and Methods

Polydimethylsiloxane (SYLGARDTM 184) was purchased from Krayden Inc., CO, USA. Glass wafer (D263, 550 µm, double side polished) was received from University Wafer, MA, USA. Magnetic beads with a diameter of 5 µm and 10 µm were ordered from Alpha Nanotech Inc, Vancouver, Canada. Magnetic beads with a diameter of 2.8 µm were purchased from Thermo Fisher Scientific, MA, USA. PBS (1× without calcium and magnesium, PH 7.4 ± 0.1) was purchased from Corning Inc, NY, USA. The fluorescent dye (*BacLight*™ Green Bacterial Stain, excitation/emission: 480/525) was obtained from Thermo Fisher Scientific. The plasma solution (P2891-10 mL) was purchased from Sigma Aldrich, MO, USA, which was diluted by the ratio of 1:10, before running experiments.

Nano-sieve device fabrication. A thin layer of TEOS was deposited onto a cleaned glass wafer with a thickness of 200 nm by using Plasma Enhanced Chemical Vapor Deposition. Then, positive resist (PR: AZ Mir 701) was spin-coated onto the TEOS layer with a thickness of ~1 µm. Standard lithography was used to pattern the nano-sieve, followed by the development process with CD-26 developer. Buffered oxide etching (BOE) was used to etch the TEOS layer, with an etching rate of ~2.72 nm/s for 75 s. Following that, PR was completely removed using the acetone solution, followed by isopropyl alcohol (IPA) rinsing for 15-20 s and then nitrogen drying. A sacrificial layer of PR was patterned in the etched channel via standard lithography. PDMS base and curing agent were mixed at a ratio of 10:1 and then cured in an oven at 85 °C for 50 mins. PDMS was casted to a final thickness of ~5 mm. The inlet and outlet holes were punched using a biopsy punch (diameter = 1 mm). Eventually, the PDMS was fused onto the fabricated glass substrate via an oxygen plasma treatment (Electro-Technic Products).

Cell culture and labeling. *Escherichia coli* (*E. coli*, ATCC 25922) cells were cultured for 14-15 hours in LB broth at 37 °C in a shaker incubator, until they reached an optical density (OD) of 0.5-0.6 measured at 600 nm, which corresponded to an approximate cell concentration of ~1.71×10^8 cells/mL. *E. coli* cells exhibited a prolate shape and were 2.38 ± 0.32 µm long and 1.20 ± 0.21 µm wide. The cells were then stained with fluorescent dye to enable visualization. Briefly, a sample of 1 mL of cell culture was centrifuged using the microcentrifuge (VWR Galaxy Mini C1213) at 2000g for 5 mins; then, the supernatant was discarded. The fresh PBS was applied in order to rinse and re-suspend the condensed cells. Subsequently, 4 µL of the *BacLight* dye was added into 1 mL of the PBS-based bacteria solution for staining the *E. coli* cells; then, the sample solution was vortexed for 10-15 s. The stained cells were incubated at room temperature for approximately 20 mins, followed by centrifugation at 2000g for 5 mins. Afterward, the supernatant was discarded, and the pellet of cells was rinsed again using fresh PBS to remove the excess dye. Finally, the cells were re-suspended in 0.5 mL of fresh PBS and ready for use in the experiment. Cell concentration expressed as CFU was determined by performing a series of dilutions of overnight liquid culture (OD = 0.92, ~2.71×10^8 cells/mL). This culture was diluted 1:10 stock/mL four consecutive times. The most diluted culture (0.0001 stock/mL) was then plated on a solid LB agar petri dish and incubated for 24 hours at 37 °C. Following growth overnight, the number of colonies was counted visually, and the resulting concentration was estimated as 1.00×10^8 CFU/mL (Refer to Table S1 in the Support Information).

Bead stacking and bacteria-trapping. A syringe pump (WPI, SP220I Syringe Pump) was used to inject magnetic beads into the nano-sieve channel. Subsequently, the bacteria solution was pumped into the channel using a syringe pump at various flow rates. The filtered waste was collected in a centrifuge tube. Afterwards, fresh PBS was applied to wash the magnetic beads and

bacteria out of the nano-sieve channel, then collected in another centrifuge tube that was held on a magnetic rack.

CFD modeling. The Eulerian multiphase model in FLUENT 19.2 was used to simulate the transport of beads through the nano-sieve. Water flow was assumed as laminar flow since the maximum Reynolds number was less than 30. Velocity inlet and pressure outlet boundary conditions were applied to the inlet and outlet. The diameter and density of the beads used in the simulation were 10 µm and 2500 kg/m^3, respectively.

Tomography scanning. Volumetric topology was evaluated via an optical coherence tomography (OCT, Thorlab, Ganymede) system. The system used a near-infrared light source (790 nm to 990 nm) to illuminate the bead sample and then measured the backscattering properties. It was a label-free process, which covered a region of $3 \times 6 \times 1.94$ mm^3. To quantitatively measure the volume of beads in each flow rate, we devised an unsupervised machine learning tool for segmentation, which integrated k-mean clustering and the critical morphological operations, to automatically extract the boundary of the bead stack within the 3D space.

Spectrofluorometric characterization. A spectrofluorometer (JASCO FP–8500) was used to measure the fluorescence intensity of the stained cells. The excitation wavelength was set at 480 nm, and the sensitivity was set at "high" level to measure all the samples in this study. Spectra analysis software (JASCO corporation) was used to collect data from the spectrofluorometer.

Fluorescence microscopy imaging. The magnetic beads and bacteria samples were imaged with a high-speed camera (AxioCam MRc, Zeiss) mounted on the microscope (AmScope). The fluorescence power source and GFP filter kit were used to visualize the *E.coli* bacteria stained by fluorescent dye. The lens magnification was set at 2.5× and 100×, with an exposure time of 100 ms.

Scanning electron microscopy (SEM). SEM (Tescan Mira3) was used to image the magnetic beads in the nano-sieve channel. Samples were mounted onto the specific holder using the copper taper. Then, ~200 nm of metal film was coated on the sample by using a sputter coater (SPI-Module™ Sputter Coater). For SEM imaging, the voltage was set at 20 kV.
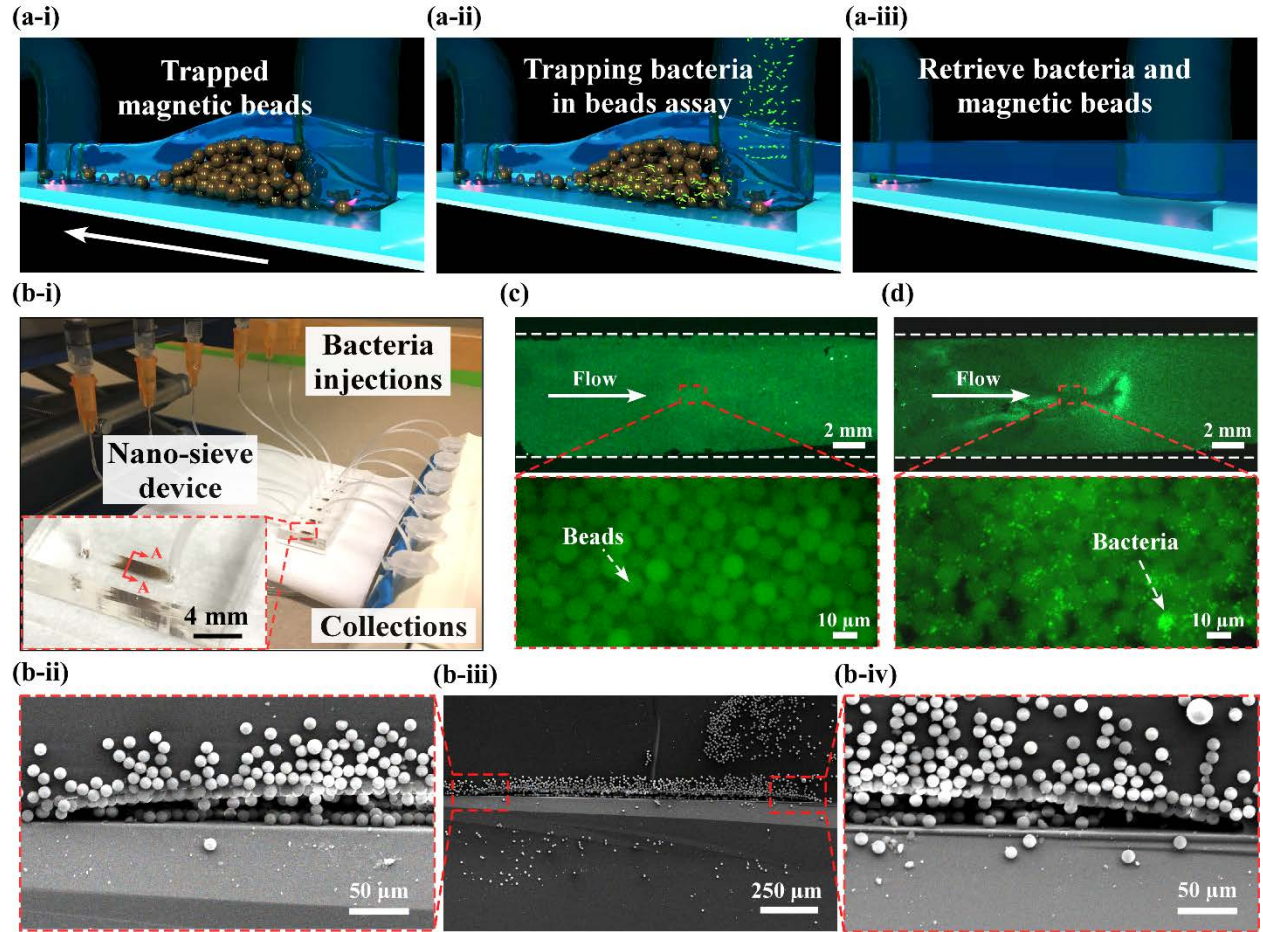
FIGURES

Figure 1. (a) Illustration of the magnetic beads stacked nano-sieve device for bacteria isolation: (i) beads trapped in the nano-sieve; (ii) pumping bacteria into the nano-sieve; (iii) bacteria retrieval via high flow rate buffer washing. (b) Magnetic beads trapping: (i) Experimental setup. Inset: photograph of beads stacked nano-sieve device. SEM images of the beads stacked nano-sieve channel: (b-ii) Left; (b-iii) Middle; (b-iv) Right. Fluorescence microscope image of the channel before (c) and after (d) bacteria-trapping. The white arrow indicates the flow direction.
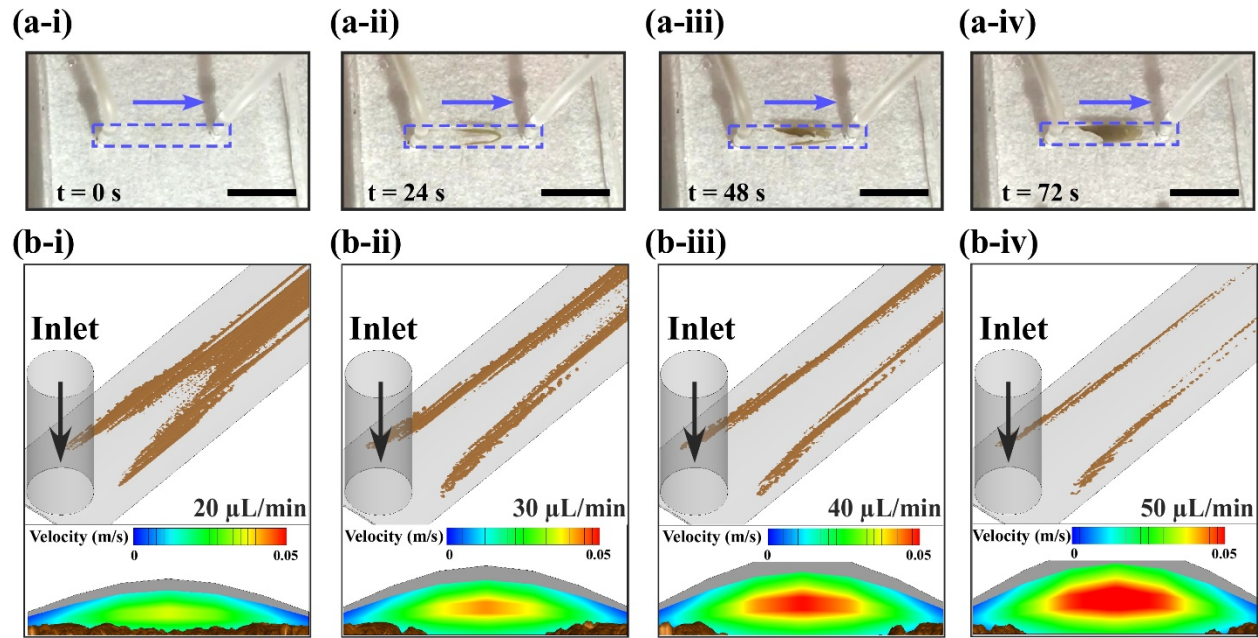
Figure 2. (a) Beads stacking process during 72 s with a flow rate of 40 µL/min. The dashed purple box indicates the channel. The arrow indicates the flow direction. Scale bar: 4 mm. (b) Top: CFD calculation of nano-sieve deformation and beads flow pattern; bottom: flow velocity with a flow rate of (i) 20 µL/min; (ii) 30 µL/min; (iii) 40 µL/min; (iv) 50 µL/min.
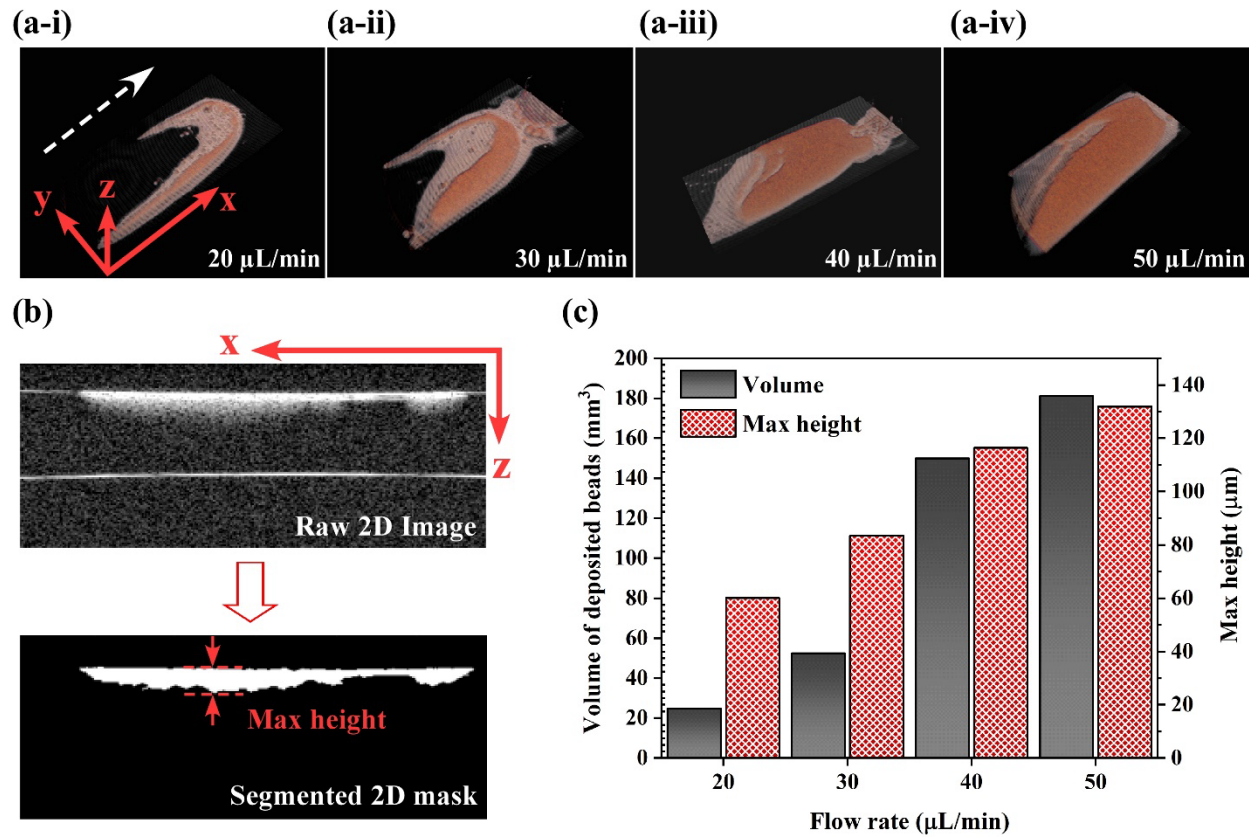
Figure 3. (a) Optical coherence tomography scan of the beads stacked nano-sieve with the flow rate ranging from 20 - 50 µL/min. (b) Cross-section view of beads stacking: raw 2D image (top) and segmented 2D mask (bottom). (c) Experientially measured volume of the deposited beads and maximum height in the channel after beads stacking.
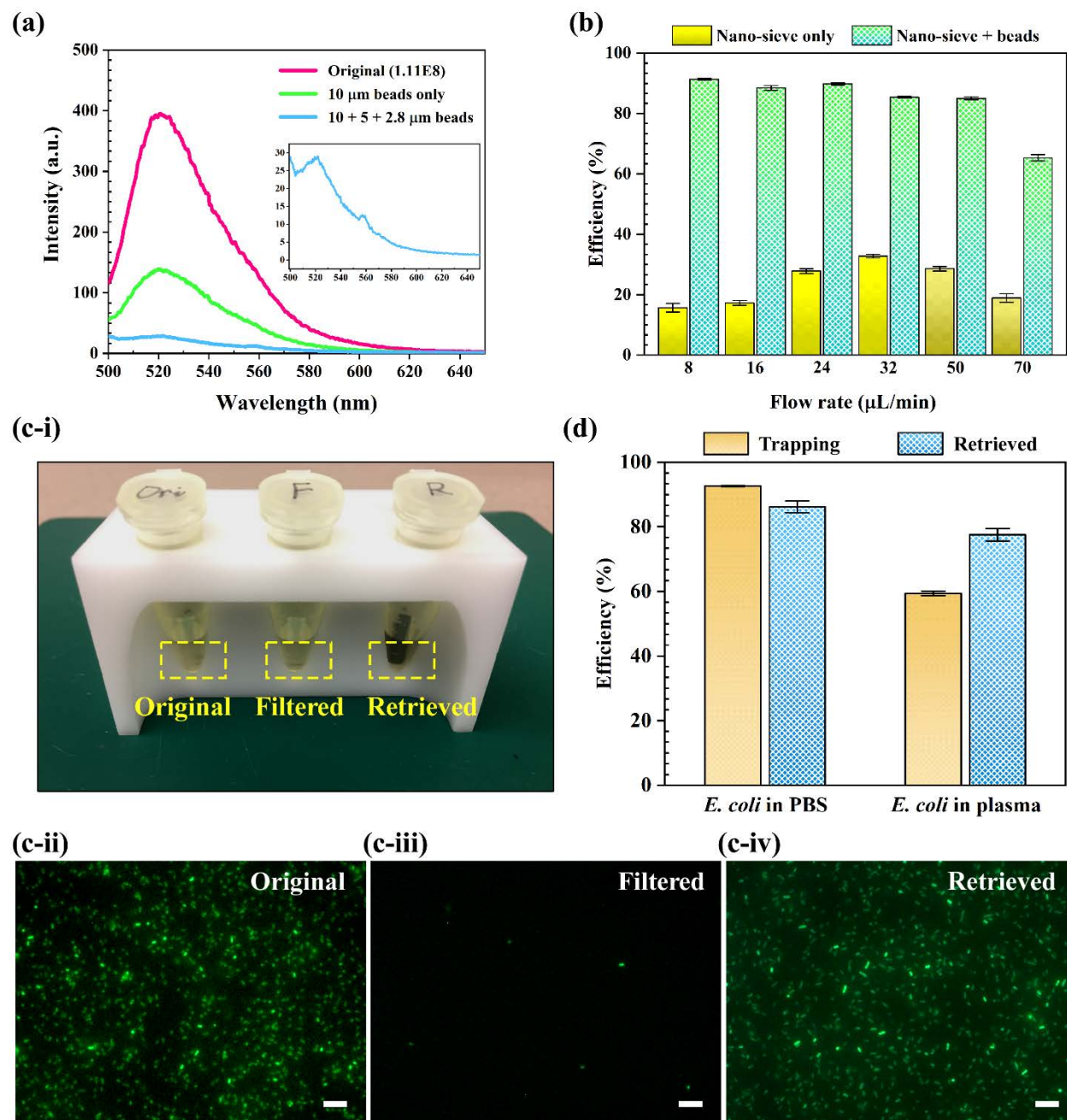
Figure 4. (a) Uncorrected emission curve of filtered solution from nano-sieve with a flow rate of 8 µL/min: Original solution (pink); Stacked with 10 µm beads (green); Stacked with mixed beads with sizes of 2.8 µm, 5 µm, and 10 µm (blue). The emission peaks are centered at ~520 nm. (b) Bacteria-trapping efficiency versus flow rate of nano-sieve only (yellow) and beads stacked nano-sieve (patterned green). (c-i) Photograph of the bacteria samples: Original (left); Filtered (middle); Retrieved (right). Fluorescence microscope image of original solution (c-ii), filtered solution (c-iii), and retrieved solution (c-iv). Scale bar: 10 µm. (d) Bacteria-trapping efficiency and retrieval efficiency from PBS (brown) and pig plasma (patterned blue). The applied flow rate is 8 µL/min. Error bars indicate standard deviation of the mean.
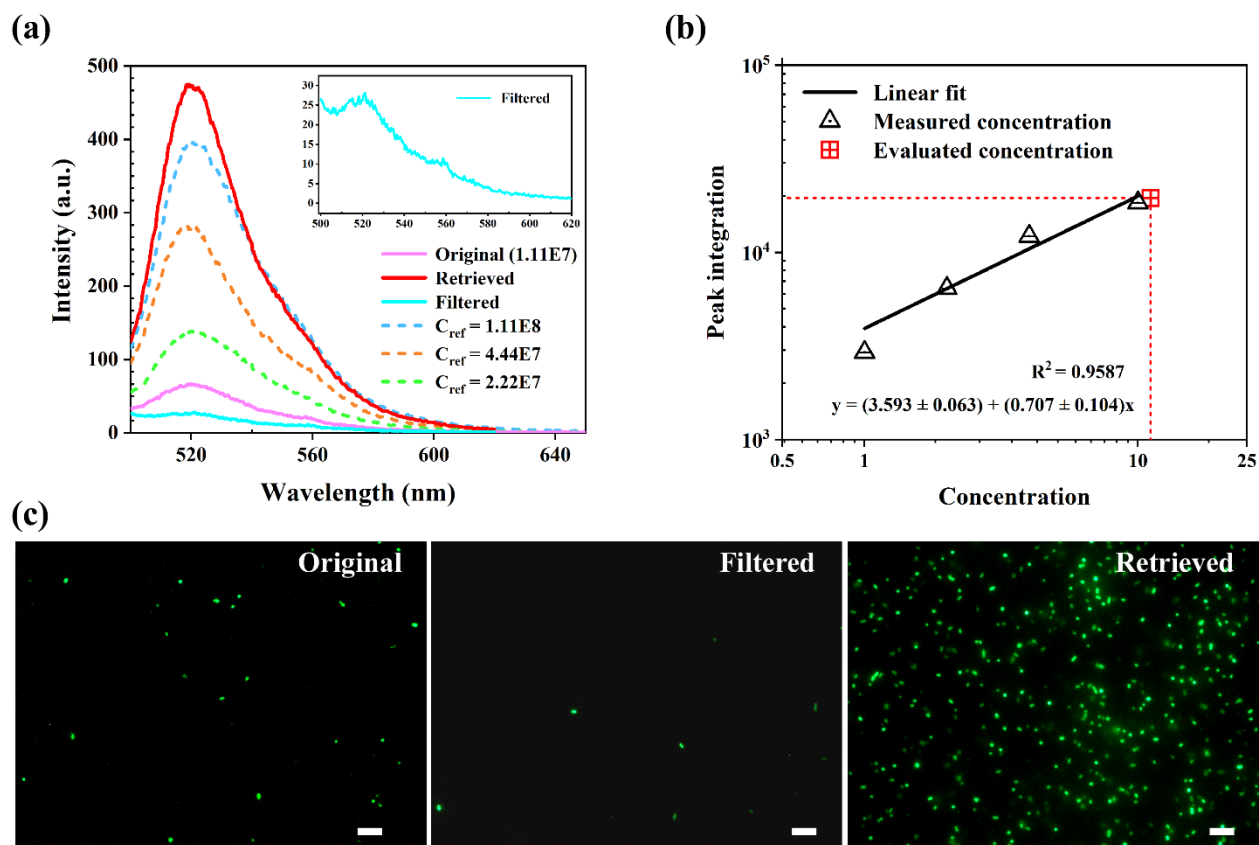
19

Figure 5. (a) Uncorrected emission curve of bacteria solution with various concentrations. The emission peak is centered at ~520 nm. The input bacteria concentration and volume are 1.11E7 CFU/mL and 1,300 µL , respectively (solid pink line). The retrieved sample is in 100 µL PBS (solid red line). Inset: Uncorrected emission curve of filtered solution. (b) Fluorescence intensity versus bacteria concentration. The estimated concentration factor is 13 and the evaluated concentration factor is ~11. Error bars are standard error of the mean. (c) Fluorescence microscope image of original solution (left); filtered solution (middle); retrieved (right). Scale bar: 10 µm.

ASSOCIATED CONTENT

Supporting information

Movie S1. Video of the beads stacking process with a flow rate of 40 µL/min. (*The file is separately stored in the folder, named by "# Stacked beads profile 0-72s - crop"*)

Stacked beads profile 0-72s - crop.avi

Table S1. Table of *E. coli* cell number counting by CFU/mL.

Number of colonies	Dilution of factor	Volume of culture plated (mL)	Initial concentration (cfu/mL)	Initial concentration (cells/mL)	Factor of division
1000	10000	0.1	1.00E+08	2.70E+08	2.70
Formula[56] of calculation	cfu/mL = (number of colonies × dilution factor) / volume of culture plate				

AUTHOR INFORMATION

Corresponding Author: ke.du@rit.edu

Present Addresses: 76 Lomb Memorial Drive, Rochester, NY 14623

(PHT180) at RIT for schematic design. Part of the nano-sieve device fabrication was conducted in The Semiconductor & Microsystems Fabrication Laboratory at RIT.

REFERENCES

(1)   Prüss-Ustün, A.; Bartram, J.; Clasen, T.; Colford, J. M.; Cumming, O.; Curtis, V.; Bonjour, S.; Dangour, A. D.; France, J. D.; Fewtrell, L.; et al. Burden of disease from inadequate water, sanitation and hygiene in low- and middle-income settings: a retrospective analysis of data from 145 countries. *Trop. Med. Int. Health* **2014**, *19* (8), 894–905. https://doi.org/10.1111/tmi.12329.

(2)   Mead, P. S.; Slutsker, L.; Dietz, V.; McCaig, L. F.; Bresee, J. S.; Shapiro, C.; Griffin, P. M.; Tauxe, R. V. Food-Related Illness and Death in the United States. *Emerg. Infect. Dis.* **1999**, *5* (5), 607–625.

(3)   Goff, D. A.; Kullar, R.; Bauer, K. A.; File, T. M. Eight Habits of Highly Effective Antimicrobial Stewardship Programs to Meet the Joint Commission Standards for Hospitals. *Clin. Infect. Dis.* **2017**, *64* (8), 1134–1139. https://doi.org/10.1093/cid/cix065.

(4)   O'neill, J. I. M. Antimicrobial Resistance: Tackling a Crisis for the Health and Wealth of Nations. *Rev Antimicrob Resist* **2014**, *20*, 1–16.

(5)   Shao, H.; Chung, J.; Lee, K.; Balaj, L.; Min, C.; Carter, B. S.; Hochberg, F. H.; Breakefield, X. O.; Lee, H.; Weissleder, R. Chip-Based Analysis of Exosomal MRNA Mediating Drug Resistance in Glioblastoma. *Nat. Commun.* **2015**, *6*, 6999.

(6)   Oshimori, N.; Oristian, D.; Fuchs, E. TGF-β Promotes Heterogeneity and Drug Resistance in Squamous Cell Carcinoma. *Cell* **2015**, *160* (5), 963–976.

(7)   Wu, W.; Li, J.; Pan, D.; Li, J.; Song, S.; Rong, M.; Li, Z.; Gao, J.; Lu, J. Gold Nanoparticle-Based Enzyme-Linked Antibody-Aptamer Sandwich Assay for Detection of Salmonella Typhimurium. *ACS Appl. Mater. Interfaces* **2014**, *6* (19), 16974–16981.

(8)   Toh, S. Y.; Citartan, M.; Gopinath, S. C.; Tang, T.-H. Aptamers as a Replacement for Antibodies in Enzyme-Linked Immunosorbent Assay. *Biosens. Bioelectron.* **2015**, *64*, 392–403.

(9)   Haaber, J.; Leisner, J. J.; Cohn, M. T.; Catalan-Moreno, A.; Nielsen, J. B.; Westh, H.; Penadés, J. R.; Ingmer, H. Bacterial Viruses Enable Their Host to Acquire Antibiotic Resistance Genes from Neighbouring Cells. *Nat. Commun.* **2016**, *7*, 13333.

(10)   Liu, X.; Painter, R. E.; Enesa, K.; Holmes, D.; Whyte, G.; Garlisi, C. G.; Monsma, F. J.; Rehak, M.; Craig, F. F.; Smith, C. A. High-Throughput Screening of Antibiotic-Resistant Bacteria in Picodroplets. *Lab. Chip* **2016**, *16* (9), 1636–1643.

(11)   Sanyasi, S.; Majhi, R. K.; Kumar, S.; Mishra, M.; Ghosh, A.; Suar, M.; Satyam, P. V.; Mohapatra, H.; Goswami, C.; Goswami, L. Polysaccharide-Capped Silver Nanoparticles Inhibit Biofilm Formation and Eliminate Multi-Drug-Resistant Bacteria by Disrupting Bacterial Cytoskeleton with Reduced Cytotoxicity towards Mammalian Cells. *Sci. Rep.* **2016**, *6*, 24929.

(12)   Koch, G.; Yepes, A.; Förstner, K. U.; Wermser, C.; Stengel, S. T.; Modamio, J.; Ohlsen, K.; Foster, K. R.; Lopez, D. Evolution of Resistance to a Last-Resort Antibiotic in Staphylococcus Aureus via Bacterial Competition. *Cell* **2014**, *158* (5), 1060–1071.

(13)   Wildt, R. M. T. de; Mundy, C. R.; Gorick, B. D.; Tomlinson, I. M. Antibody Arrays for High-Throughput Screening of Antibody–Antigen Interactions. *Nat. Biotechnol.* **2000**, *18* (9), 989–994. https://doi.org/10.1038/79494.

(14) Tajima, N.; Takai, M.; Ishihara, K. Significance of Antibody Orientation Unraveled: Well-Oriented Antibodies Recorded High Binding Affinity. *Anal. Chem.* **2011**, *83* (6), 1969–1976. https://doi.org/10.1021/ac1026786.

(15) García-Fernández, E.; Koch, G.; Wagner, R. M.; Fekete, A.; Stengel, S. T.; Schneider, J.; Mielich-Süss, B.; Geibel, S.; Markert, S. M.; Stigloher, C. Membrane Microdomain Disassembly Inhibits MRSA Antibiotic Resistance. *Cell* **2017**, *171* (6), 1354-1367. e20.

(16) Nebe-von-Caron, G.; Stephens, P. J.; Hewitt, C. J.; Powell, J. R.; Badley, R. A. Analysis of Bacterial Function by Multi-Colour Fluorescence Flow Cytometry and Single Cell Sorting. *J. Microbiol. Methods* **2000**, *42* (1), 97–114.

(17) Stark, R. P.; Maki, D. G. Bacteriuria in the Catheterized Patient: What Quantitative Level of Bacteriuria Is Relevant? *N. Engl. J. Med.* **1984**, *311* (9), 560–564.

(18) Beattie, W.; Qin, X.; Wang, L.; Ma, H. Clog-Free Cell Filtration Using Resettable Cell Traps. *Lab. Chip* **2014**, *14* (15), 2657–2665.

(19) Liu, C.; Mauk, M.; Gross, R.; Bushman, F. D.; Edelstein, P. H.; Collman, R. G.; Bau, H. H. Membrane-Based, Sedimentation-Assisted Plasma Separator for Point-of-Care Applications. *Anal. Chem.* **2013**, *85* (21), 10463–10470. https://doi.org/10.1021/ac402459h.

(20) Hong, S. C.; Kang, J. S.; Lee, J. E.; Kim, S. S.; Jung, J. H. Continuous Aerosol Size Separator Using Inertial Microfluidics and Its Application to Airborne Bacteria and Viruses. *Lab. Chip* **2015**, *15* (8), 1889–1897.

(21) Shen, S.; Tian, C.; Li, T.; Xu, J.; Chen, S.-W.; Tu, Q.; Yuan, M.-S.; Liu, W.; Wang, J. Spiral Microchannel with Ordered Micro-Obstacles for Continuous and Highly-Efficient Particle Separation. *Lab. Chip* **2017**, *17* (21), 3578–3591.

(22) Kuan, D.-H.; Wu, C.-C.; Su, W.-Y.; Huang, N.-T. A Microfluidic Device for Simultaneous Extraction of Plasma, Red Blood Cells, and On-Chip White Blood Cell Trapping. *Sci. Rep.* **2018**, *8* (1), 1–9. https://doi.org/10.1038/s41598-018-33738-8.

(23) Ishikawa, T.; Shioiri, T.; Numayama-Tsuruta, K.; Ueno, H.; Imai, Y.; Yamaguchi, T. Separation of Motile Bacteria Using Drift Velocity in a Microchannel. *Lab. Chip* **2014**, *14* (5), 1023–1032. https://doi.org/10.1039/C3LC51302E.

(24) Rudisch, B. M.; Pfeiffer, S. A.; Geissler, D.; Speckmeier, E.; Robitzki, A. A.; Zeitler, K.; Belder, D. Nonaqueous Micro Free-Flow Electrophoresis for Continuous Separation of Reaction Mixtures in Organic Media. *Anal. Chem.* **2019**, *91* (10), 6689–6694. https://doi.org/10.1021/acs.analchem.9b00714.

(25) Wang, Z.-F.; Cheng, S.; Ge, S.-L.; Wang, H.; Wang, Q.-J.; He, P.-G.; Fang, Y.-Z. Ultrasensitive Detection of Bacteria by Microchip Electrophoresis Based on Multiple-Concentration Approaches Combining Chitosan Sweeping, Field-Amplified Sample Stacking, and Reversed-Field Stacking. *Anal. Chem.* **2012**, *84* (3), 1687–1694.

(26) Ohlsson, P.; Evander, M.; Petersson, K.; Mellhammar, L.; Lehmusvuori, A.; Karhunen, U.; Soikkeli, M.; Seppä, T.; Tuunainen, E.; Spangar, A. Integrated Acoustic Separation, Enrichment, and Microchip Polymerase Chain Reaction Detection of Bacteria from Blood for Rapid Sepsis Diagnostics. *Anal. Chem.* **2016**, *88* (19), 9403–9411.

(27) Ai, Y.; Sanders, C. K.; Marrone, B. L. Separation of Escherichia Coli Bacteria from Peripheral Blood Mononuclear Cells Using Standing Surface Acoustic Waves. *Anal. Chem.* **2013**, *85* (19), 9126–9134. https://doi.org/10.1021/ac4017715.

(28) A. Kulkarni, J.; C. Tam, Y. Y.; Chen, S.; K. Tam, Y.; Zaifman, J.; R. Cullis, P.; Biswas, S. Rapid Synthesis of Lipid Nanoparticles Containing Hydrophobic Inorganic Nanoparticles. *Nanoscale* **2017**, *9* (36), 13600–13609. https://doi.org/10.1039/C7NR03272B.

(29) Fanalista, F.; Birnie, A.; Maan, R.; Burla, F.; Charles, K.; Pawlik, G.; Deshpande, S.; Koenderink, G. H.; Dogterom, M.; Dekker, C. Shape and Size Control of Artificial Cells for Bottom-Up Biology. *ACS Nano* **2019**, *13* (5), 5439–5450. https://doi.org/10.1021/acsnano.9b00220.

(30) Zeming, K. K.; Ranjan, S.; Zhang, Y. Rotational Separation of Non-Spherical Bioparticles Using I-Shaped Pillar Arrays in a Microfluidic Device. *Nat. Commun.* **2013**, *4*, 1625. https://doi.org/10.1038/ncomms2653.

(31) Huang, L. R. Continuous Particle Separation Through Deterministic Lateral Displacement. *Science* **2004**, *304* (5673), 987–990. https://doi.org/10.1126/science.1094567.

(32) Campos, M.; Surovtsev, I. V.; Kato, S.; Paintdakhi, A.; Beltran, B.; Ebmeier, S. E.; Jacobs-Wagner, C. A Constant Size Extension Drives Bacterial Cell Size Homeostasis. *Cell* **2014**, *159* (6), 1433–1446. https://doi.org/10.1016/j.cell.2014.11.022.

(33) Chen, X.; Falzon, L.; Zhang, J.; Zhang, X.; Wang, R.-Q.; Du, K. Experimental and Theoretical Study on the Microparticle Trapping and Release in a Deformable Nano-Sieve Channel. *Nanotechnology* **2019**. https://doi.org/10.1088/1361-6528/ab2279.

(34) Gan, Y.; Tsay, D.; Amir, S. B.; Marboe, C. C.; Hendon, C. P. Automated Classification of Optical Coherence Tomography Images of Human Atrial Tissue. *J. Biomed. Opt.* **2016**, *21* (10), 101407.

(35)   Dobe, O.; Sarkar, A.; Halder, A. Rough K-Means and Morphological Operation-Based Brain Tumor Extraction. In *Integrated Intelligent Computing, Communication and Security*; Springer, 2019; pp 661–667.

(36)   Apisarnthanarak, A.; Tunpornchai, J.; Tanawitt, K.; Mundy, L. M. Nonjudicious Dispensing of Antibiotics by Drug Stores in Pratumthani, Thailand. *Infect. Control Hosp. Epidemiol.* **2008**, *29* (6), 572–575. https://doi.org/10.1086/587496.

(37)   Abahussain, N. A.; Taha, A. Z. Knowledge and Attitudes of Female School Students on Medications in Eastern Saudi Arabia. *Saudi Med. J.* **2007**, *28* (11), 1723.

(38)   Micek, S. T.; Welch, E. C.; Khan, J.; Pervez, M.; Doherty, J. A.; Reichley, R. M.; Kollef, M. H. Empiric Combination Antibiotic Therapy Is Associated with Improved Outcome against Sepsis Due to Gram-Negative Bacteria: A Retrospective Analysis. *Antimicrob. Agents Chemother.* **2010**, *54* (5), 1742–1748. https://doi.org/10.1128/AAC.01365-09.

(39)   Hill, V. R.; Polaczyk, A. L.; Hahn, D.; Narayanan, J.; Cromeans, T. L.; Roberts, J. M.; Amburgey, J. E. Development of a Rapid Method for Simultaneous Recovery of Diverse Microbes in Drinking Water by Ultrafiltration with Sodium Polyphosphate and Surfactants. *Appl Env. Microbiol* **2005**, *71* (11), 6878–6884.

(40)   Zheng, X. T.; Tan, Y. N. Development of Blood-Cell-Selective Fluorescent Biodots for Lysis-Free Leukocyte Imaging and Differential Counting in Whole Blood. *Small* **2019**. https://doi.org/10.1002/smll.201903328.

(41)   Su, X.-L.; Li, Y. Quantum Dot Biolabeling Coupled with Immunomagnetic Separation for Detection of Escherichia Coli O157:H7. *Anal. Chem.* **2004**, *76* (16), 4806–4810. https://doi.org/10.1021/ac049442+.

(42)   Malic, L.; Zhang, X.; Brassard, D.; Clime, L.; Daoud, J.; Luebbert, C.; Barrere, V.; Boutin, A.; Bidawid, S.; Farber, J.; et al. Polymer-Based Microfluidic Chip for Rapid and Efficient Immunomagnetic Capture and Release of Listeria Monocytogenes. *Lab. Chip* **2015**, *15* (20), 3994–4007. https://doi.org/10.1039/C5LC00852B.

(43)   Narayan, R. J. *Medical Biosensors for Point of Care (POC) Applications*; Woodhead Publishing, 2016.

(44)   Ohlsson, P.; Petersson, K.; Augustsson, P.; Laurell, T. Acoustic Impedance Matched Buffers Enable Separation of Bacteria from Blood Cells at High Cell Concentrations. *Sci. Rep.* **2018**, *8* (1), 9156.

(45)   Kye, H. G.; Park, B. S.; Lee, J. M.; Song, M. G.; Song, H. G.; Ahrberg, C. D.; Chung, B. G. Dual-Neodymium Magnet-Based Microfluidic Separation Device. *Sci. Rep.* **2019**, *9* (1), 1–10. https://doi.org/10.1038/s41598-019-45929-y.

(46)   Li, P.; Huang, T. J. Applications of Acoustofluidics in Bioanalytical Chemistry. *Anal. Chem.* **2019**, *91* (1), 757–767. https://doi.org/10.1021/acs.analchem.8b03786.

(47)   Cheng, Y.; Wang, Y.; Ma, Z.; Wang, W.; Ye, X. A Bubble-and Clogging-Free Microfluidic Particle Separation Platform with Multi-Filtration. *Lab. Chip* **2016**, *16* (23), 4517–4526.

(48)   Yoon, Y.; Kim, S.; Lee, J.; Choi, J.; Kim, R.-K.; Lee, S.-J.; Sul, O.; Lee, S.-B. Clogging-Free Microfluidics for Continuous Size-Based Separation of Microparticles. *Sci. Rep.* **2016**, *6*, 26531.

(49)   Jin, Z.; Sun, W.; Ke, Y.; Shih, C.-J.; Paulus, G. L.; Wang, Q. H.; Mu, B.; Yin, P.; Strano, M. S. Metallized DNA Nanolithography for Encoding and Transferring Spatial Information for Graphene Patterning. *Nat. Commun.* **2013**, *4*, 1663.

(50)   Kim, S.; Marelli, B.; Brenckle, M. A.; Mitropoulos, A. N.; Gil, E.-S.; Tsioris, K.; Tao, H.; Kaplan, D. L.; Omenetto, F. G. All-Water-Based Electron-Beam Lithography Using Silk as a Resist. *Nat. Nanotechnol.* **2014**, *9* (4), 306.

(51)   Lebleu, N.; Roques, C.; Aimar, P.; Causserand, C. Role of the Cell-Wall Structure in the Retention of Bacteria by Microfiltration Membranes. *J. Membr. Sci.* **2009**, *326* (1), 178–185. https://doi.org/10.1016/j.memsci.2008.09.049.

(52)   Zydney, A. L.; Saltzman, W. M.; Colton, C. K. Hydraulic Resistance of Red Cell Beds in an Unstirred Filtration Cell. *Chem. Eng. Sci.* **1989**, *44* (1), 147–159.

(53)   Ahmed, T.; Shimizu, T. S.; Stocker, R. Microfluidics for Bacterial Chemotaxis. *Integr. Biol.* **2010**, *2* (11–12), 604–629. https://doi.org/10.1039/c0ib00049c.

(54)   Beebe, D. J.; Mensing, G. A.; Walker, G. M. Physics and Applications of Microfluidics in Biology. *Annu. Rev. Biomed. Eng.* **2002**, *4* (1), 261–286.

(55)   Gu, H.; Ho, P.-L.; Tsang, K. W. T.; Wang, L.; Xu, B. Using Biofunctional Magnetic Nanoparticles to Capture Vancomycin-Resistant Enterococci and Other Gram-Positive Bacteria at Ultralow Concentration. *J. Am. Chem. Soc.* **2003**, *125* (51), 15702–15703. https://doi.org/10.1021/ja0359310.

(56)   Pollack, R. A.; Findlay, L.; Mondschein, W.; Modesto, R. R. *Laboratory Exercises in Microbiology*; John Wiley & Sons, 2012.